ACS Energy LETTERS

http://pubs.acs.org/journal/aelccp

Deciphering Unresolved Materials in Quantitative Analysis of Lithium Metal Solid Electrolyte Interphases

Katherine Steinberg, Wurigumula Bao, Kun Ryu, Ying Shirley Meng, and Betar M. Gallant*

Cite This: *ACS Energy Lett.* 2025, 10, 4269−4276

Read Online

ACCESS | Metrics & More | Article Recommendations | Supporting Information

ABSTRACT: Integrated quantification of inactive Li^0 and Solid Electrolyte Interphase (SEI) materials is a powerful tool to understand Coulombic inefficiency of Li metal anodes, but current approaches cannot distinguish unresolved SEI phases from materials lost during cycling or sample preparation. Here, the significance of these previously unresolvable materials was investigated in four electrolytes, leveraging gas chromatography, inductively coupled plasma atomic emission spectroscopy, and nuclear magnetic resonance. Li^0 and SEI losses were tracked across the Cu electrode, separator, and wash solvent, bringing the inventoried Li within error of the electrochemical capacity loss. Ultimately, tracking all irreversible Li in the cell did not impact relative trends in inactive Li^0 formation or SEI composition across electrolytes. This work demonstrates the robustness of capacity loss analysis to minor losses of material during sample processing, validating simpler approaches for cross-electrolyte comparison while offering a procedure for cases requiring highly precise material inventory.

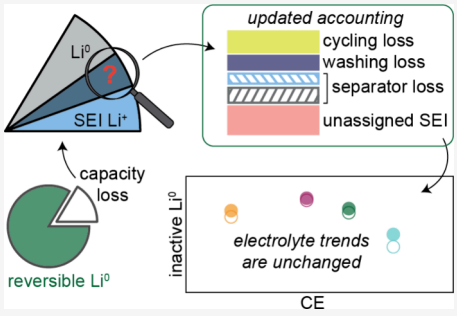

Coulombic efficiency (CE) is the key performance metric for characterizing Li anode cycling capability and increasing it has been the major aim of electrolyte design strategies spanning decades.[1] While useful for simple performance comparisons, CE and its complement, Coulombic inefficiency (1 − CE), are only gross measures of how capacity is partitioned between reversible and irreversible Li, respectively. They do not contain mechanistic information about the underlying source(s) of irreversibility, which can be several: (1) Li^0 that becomes electronically isolated, and thus is not successfully stripped from the electrode ("inactive Li^0"); (2) Solid Electrolyte Interphase (SEI) material that adheres to the working electrode ("SEI Li^+") following stripping; and (3) soluble or mechanically disconnected material produced during cycling or handling that leaves the electrode surface altogether[2−4] (Scheme 1). Recognizing this gap, in recent years, the field has developed analytical techniques, including several that employ titration, that begin to allow the Coulombic inefficiency to be quantitatively traced to specific origins, yielding the missing information about drivers of capacity loss.

Analytical techniques for Li Coulombic inefficiency quantify loss modes by selectively reacting or dissolving the solid materials that accumulate on the Cu working electrode (WE) during cycling of a Li−Cu half-cell. The reaction products are then quantified via gas chromatography (GC), mass spectrometry (MS), nuclear magnetic resonance (NMR) or ultraviolet−visible spectroscopy (UV−vis) using a suitable calibration curve.[5−7] This analysis is performed after fully stripping the Cu WE, so the remaining materials on the surface consist of electronically isolated, inactive Li^0 and insoluble SEI, *i.e.* materials relevant to capacity loss modes (1) and (2) above, which here will be called "residuals". Inactive Li^0 can be quantified by reacting residuals with water−as was originally demonstrated in foundational work by Fang *et al*[5]−or with another protic species (HA) such as acid[6,8] or alcohol,[7,9] all of which selectively generate hydrogen gas according to the following reaction:

$$2Li^0 + 2HA \rightarrow 2LiA + H_2$$

Following direct quantification of inactive Li^0, the capacity loss partitioned to SEI Li^+ is inferred by

$$SEI\ Li^+ = total\ capacity\ loss - inactive\ Li^0$$

Received: April 25, 2025
Revised: July 1, 2025
Accepted: July 30, 2025

https://doi.org/10.1021/acsenergylett.5c01274
ACS Energy Lett. 2025, 10, 4269−4276

Scheme 1. Partitioning of Capacity during Li Metal Anode Cycling and Subsequent Quantitative Capacity Loss Analysis[a]

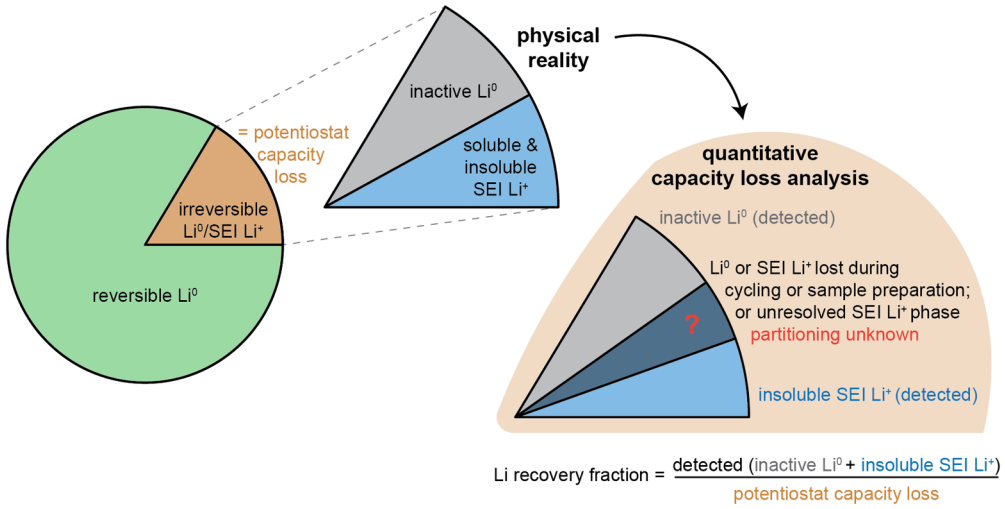

[a]Physically, irreversible capacity can consist of inactive Li^0 or SEI Li^+. Quantitative capacity loss analysis can be complicated by "missing material" with unknown partitioning.

Scheme 2. Process for Sample Preparation When Conducting Material Analyses That Require Sample Washing (Steps 1-3), and Possible Mechanisms by Which Li Residuals Could Be Lost (a-c)

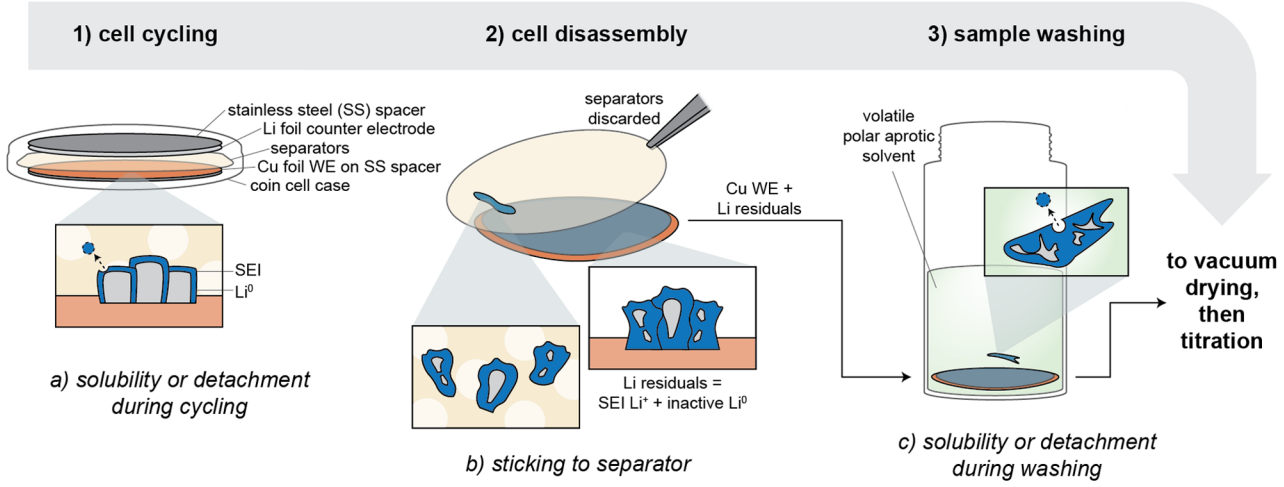

which assumes that losses (1) and (2) above are dominant and (3) is negligible. (It will be shown later that this is generally a sound assumption when Li^0 is the phase of interest). Since its development, inactive Li^0 quantification has seen increased use as a diagnostic tool for analysis of Li metal anode losses[10−18] and other anode materials like graphite, Si, and Na.[9,19−23]

Quantitative methods have also been developed to chemically resolve the identity of particular SEI materials. McShane et al. demonstrated selective detection of alkyl carbonates ($ROCO_2Li$) and lithium carbide (Li_2C_2) on graphite anodes by reacting SEI with acid, rather than water, to selectively form quantifiable gases (CO_2 and C_2H_2, respectively).[8] In previous work, a subset of the authors adapted this technique to Li metal anodes and added complementary, parallelized analytical methods, including ^{19}F-NMR in water to measure SEI lithium fluoride (LiF) content; a Karl Fischer (KF) titration in butoxyethanol to measure SEI lithium oxide (Li_2O) content; inductively coupled plasma atomic emission spectroscopy (ICP-AES) in acid or water to conduct elemental quantification on phosphorus, sulfur, and boron-derived phases and the total amount of Li-containing phases; and a colorimetric salicylate assay to measure SEI lithium nitride (Li_3N) content.[6,7] These measurements enabled a statistical analysis of the correlation between quantifiable SEI species and Coulombic efficiency (CE), revealing that Li_2O in particular is highly correlated with CE.[7]

Despite the individual power of a given analytical method, the effort to ever-more completely map capacity loss by integrating titrations for inactive Li^0 with techniques for SEI analysis presents certain important considerations. First, even for methods with high sensitivity, the inability to chemically resolve every possible SEI phase means that there is usually a shortfall—in some cases quite significant—when comparing the resolvable capacity loss to that measured by the potentiostat.[7] Without further care, this "unattributable capacity loss" cannot be successfully assigned between soluble or physically detached material lost from the electrode during cycling/sample handling, or an SEI phase that escapes chemical analysis (Scheme 1). Consequently, the mechanistic origin of these types of losses are currently unresolvable.

https://doi.org/10.1021/acsenergylett.5c01274
ACS Energy Lett. 2025, 10, 4269−4276

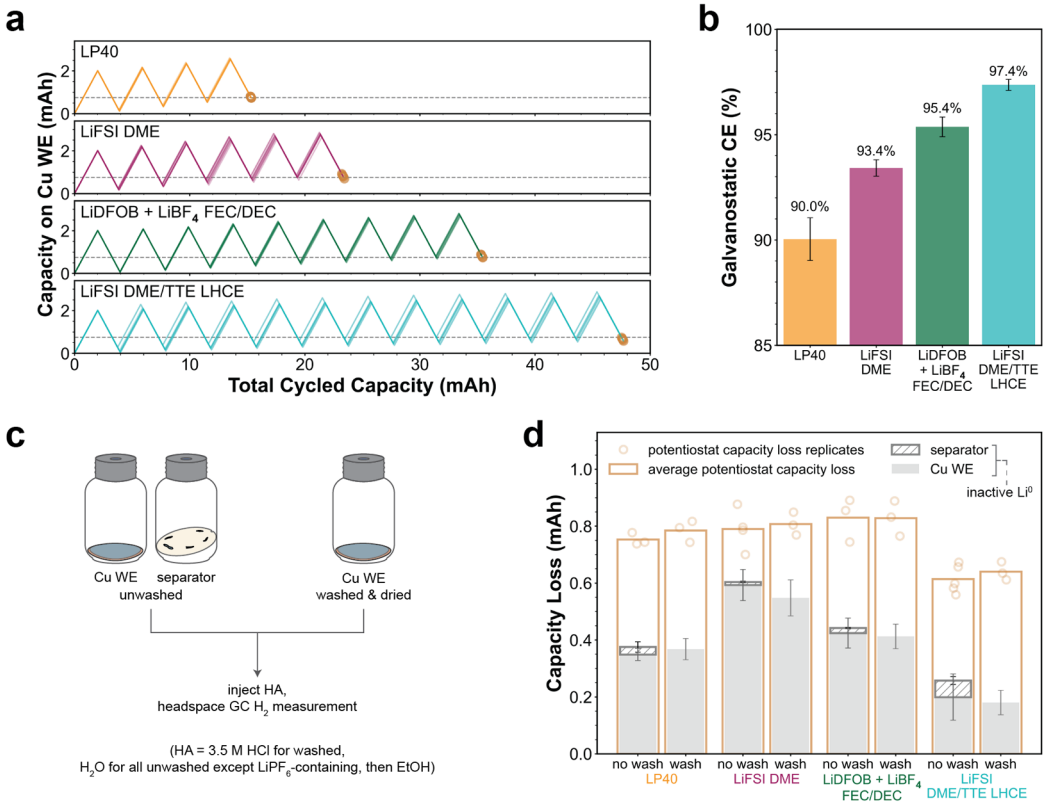

Figure 1. Impact of separator removal and washing on inactive Li^0 quantification in four exemplar electrolytes. (a) Capacity evolution during galvanostatic cycling for each electrolyte, plotted as the capacity deposited on the Cu WE vs. the total cycled capacity. The final capacity loss measured by the potentiostat for each cell is marked with a tan circle, and dashed lines denote the target capacity loss. (b) Average galvanostatic CE for each electrolyte. (c) Schematic of the procedure used for measuring inactive Li^0. (d) Inactive Li^0 measurements on unwashed vs washed samples, with the separator contribution to the total inactive Li^0 measured explicitly. The tan bar outlines show the average potentiostat capacity loss across multiple replicates, which are shown using tan circles, and gray bars mark inactive Li^0 quantity (Hatched: unwashed separator. Solid: Cu WE). For (b) and (d), bar heights mark mean values and error bars are one standard deviation, $n \geq 3$.

Second, it is conventional to normalize measured quantities of capacity loss to facilitate comparisons across electrolytes for different cycling conditions, but there are several options for normalization, which may affect the resulting numerical percentage of certain capacity loss modes shown in Scheme 1. Here, we seek to test the significance of these issues systematically, so that their relative impacts on capacity loss analysis can be better evaluated.

To begin, it is important to recognize the sample processing mandated when SEI analysis is of interest (Figure S1) and identify points at which residuals could be lost (Scheme 2). Here, the sample is usually the Cu WE from a Li−Cu half-cell and perhaps the separator closest to it. The key question in determining the necessary degree of processing is whether electrolyte residue on the sample would chemically interfere with the analytical method to be used; if yes, the electrolyte must be removed by washing. In general, it is preferable not to wash samples to minimize sample handling. However, washing is required before ICP analysis (used for total Li inventory and P, S, or B elemental quantification), because in this elemental analysis technique, electrolyte salt residue is indistinguishable from materials that are integrally part of the SEI; when quantifying alkyl carbonate SEI phases in carbonate electrolytes, because carbonate solvents react with acid to directly generate CO_2,[8] interfering with the desired signal from the alkyl carbonates themselves; and when quantifying any SEI species in the presence of salts such as $LiPF_6$, $LiBF_4$, and $LiAsF_6$ that can hydrolyze to form HF, which attacks SEI species and can produce LiF and CO_2 artifacts.[24] Therefore, in SEI analysis, washing is the rule rather than the exception; only quantification of inactive Li^0 and Li_2O do not strictly require it, because organic electrolytes do not react with acid to yield H_2 and are also generally nonreactive in KF titration, respectively[5,7] (Figure S1). An additional consideration is that inactive Li^0 and Li_2O analyses usually involve titration of the Cu electrode with its separator, because this minimizes risks of handling by peeling the electrode and separator apart. However, in cases where sample washing *is* necessary, even gentle rinsing usually dislodges the separator from the sample such that any residuals attached to the separator are lost. Thus, SEI titration analysis misses possible materials on the separator (Figure S2) unless special efforts are taken. Overall, processing steps needed for SEI analysis introduce possible additional modes of material loss compared to inactive Li^0 analysis (Scheme 2) that are important to understand.

To examine the significance of separator removal and washing steps, we investigated Li residual accounting in four disparate electrolytes: a conventional carbonate electrolyte, 1 M lithium hexafluorophosphate in ethylene carbonate/diethyl carbonate 1:1 v/v (LP40); a common ether-based electrolyte, 1 M lithium bis(fluorosulfonyl)imide in 1,2-dimethoxyethane (LiFSI DME); a dual-salt electrolyte, 1 M lithium difluoro-

https://doi.org/10.1021/acsenergylett.5c01274
ACS Energy Lett. 2025, 10, 4269−4276

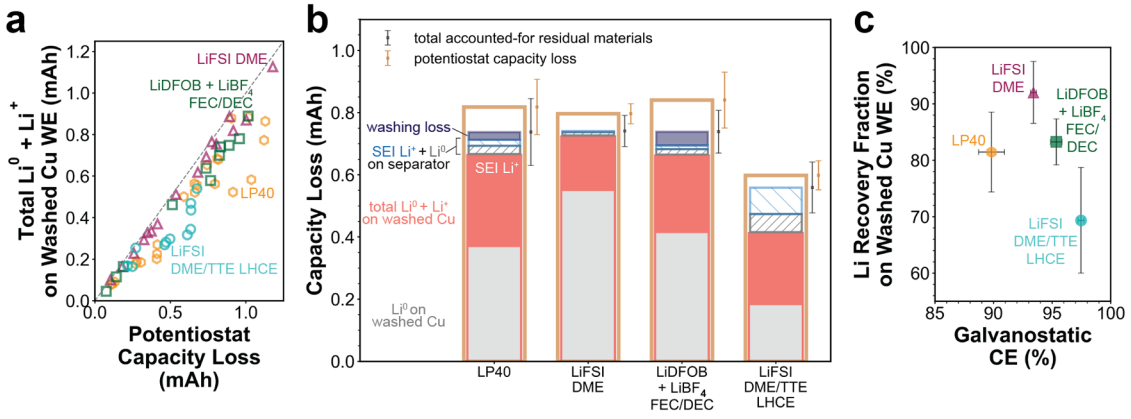

Figure 2. Impact of separator removal and washing on total Li and SEI Li^+inventory. (a) ICP measurements of combined Li^0/Li^+ inventory on washed Cu WE plotted as a function of total potentiostat capacity loss for each electrolyte, with varying capacity loss achieved by changing the total number of galvanostatic cycles. Colors/symbols correspond to the different electrolytes: orange hexagons for LP40, fuchsia triangles for LiFSI DME, green squares for LiDFOB + $LiBF_4$ FEC/DEC, and cyan circles for LiFSI DME/TTE LHCE. (b) The recovered Li inventory on washed Cu WE in each electrolyte, including total Li^0+Li^+ measured by ICP (salmon bars) and inactive Li^0 (gray bars), as well as several documented modes by which material was lost from washed WE. These include losses of inactive Li^0 to the separator (gray hatched bars), estimated losses of SEI Li^+ to the separator (blue hatched bars), and Li^+ lost to washing (purple bars). Black error bars to the right of each bar show the total propagated error from all accounted-for residuals, while the tan outlines and tan error bars show the mean and one standard deviation, respectively, in potentiostat capacity loss. For all data, $n \geq 3$. For an expanded version of this plot including error bars for individual phases, see Figure S9. (c) Average Li recovery fraction plotted vs. average galvanostatic CE for each electrolyte, with error bars marking one standard deviation, $n \geq 3$. Color and symbol assignments for each electrolyte are the same in (a).

(oxalato)borate + 0.2 M lithium tetrafluoroborate in fluoroethylene carbonate/diethyl carbonate 1:2 v/v (LiDFOB + $LiBF_4$ FEC/DEC),[25] and an ether-based localized high concentration electrolyte, LiFSI/DME/TTE (1,1,2,2-tetrafluoroethyl-2,2,3,3-tetrafluoropropylether) mixed at 1:1.2:3 molar ratios (LiFSI DME/TTE LHCE).[26] Li−Cu half cells were cycled galvanostatically at 0.5 mA cm^{-2} with 1.0 mAh cm^{-2} capacity, varying the total number of cycles between different electrolytes to achieve total capacity losses of approximately 0.6 − 0.8 mAh in all samples (Figure 1a, Figure S3, Note S1). LP40 has the lowest average CE (90.0%), followed by LiFSI DME (93.4%), LiDFOB + $LiBF_4$ FEC/DEC (95.4%), and LiFSI DME/TTE LHCE (97.4%) (Figure 1b).

After cycling, cells were disassembled and samples were either left unwashed, saving the separator closest to the Cu WE for titration (cells contained two separators); or were washed, discarding the separators. Each sample contained either the Cu WE or separator from a single coin cell, which was cycled as described above to accumulate 0.6 − 0.8 mAh of capacity loss, equivalent to ∼ 22 − 30 μmol of combined inactive Li^0 and SEI Li^+ (Figure S4). Inactive Li^0 quantification was then performed on the unwashed Cu WE and unwashed separator, or washed Cu WE alone (Figure 1c). Across all four electrolytes, the total quantity of inactive Li^0 on unwashed samples was within error of that on washed samples, despite a reliably nonzero but comparatively small quantity of inactive Li^0 detected on the separators; this finding was quantitatively reproducible across both of the authors' laboratories (Figure S5). Interestingly, the LiFSI DME electrolyte generated the greatest total amount of inactive Li^0 overall, but had the least inactive Li^0 in the separator, while the electrolyte that generated the least inactive Li^0 had the most stuck to the separator (LiFSI DME/TTE LHCE) (Figure S6). While the partitioning of minor amounts of inactive Li^0 to the separator appears chemistry-dependent, this experiment strongly suggests that washing and disassembly do not significantly influence conclusions related to inactive Li^0.

Figure 1d makes apparent, however, that there is still a large difference (indicated by the white region of each bar) between the inventoried Li^0 and the total capacity loss measured by the potentiostat. Without further information, this difference might be assumed to be entirely insoluble SEI material (as in Scheme 1); in that case the total amount of irreversible Li (Li^+ + Li^0) present on Cu, measured via ICP or NMR quantification, would be identical to the potentiostat capacity loss. Figure 2 shows the results of such ICP analysis on washed Cu electrodes for the four examined electrolytes. As we have also reported previously,[6] the Li^0/Li^+ inventory accumulates fairly linearly with cycling (Figure 2a), but in no case is the measured total Li inventory identical to potentiostat capacity loss. Specifically, the quantity of missing material ranged from <0.05 mAh (LiFSI DME, for samples with a capacity loss of ∼ 0.8 mAh) to ∼ 0.2 mAh (LiFSI DME/TTE LHCE, for samples with a capacity loss of ∼ 0.6 mAh) (Figure 2b). This yields a Li recovery fraction,

$$\mathcal{R} = \frac{Li\ residuals\ measured\ on\ washed\ Cu\ WE\ [mAh]}{potentiostat\ capacity\ loss\ [mAh]}$$

that varies substantially between electrolytes: LiFSI DME has the highest value of 93.5 ± 4.9%, followed by LiDFOB + $LiBF_4$ FEC/DEC at 83.3 ± 4.1%, LP40 at 80.6 ± 7.2%, and LiFSI DME/TTE at 69.4 ± 9.4% (Figure 2c). The recovery fraction does not exhibit a clear trend with CE. Thus, although high-CE electrolytes are typically observed to promote denser, more compact Li deposit morphology (Figure S7), high-CE morphology does not prevent material loss from the sample during cycling or washing and disassembly.

The difference between Li inventory and potentiostat capacity loss in Figure 2b defines a major dilemma in titration analyses: unclear partitioning of unaccounted-for material in washed samples used for SEI analysis (dark blue wedge in Scheme 1). The inactive Li^0 lost to the separator (Figure 1d, and included in Figure 2b) accounts for a small part of this gap, but the impact of separator removal can be more completely

https://doi.org/10.1021/acsenergylett.5c01274
ACS Energy Lett. 2025, 10, 4269−4276

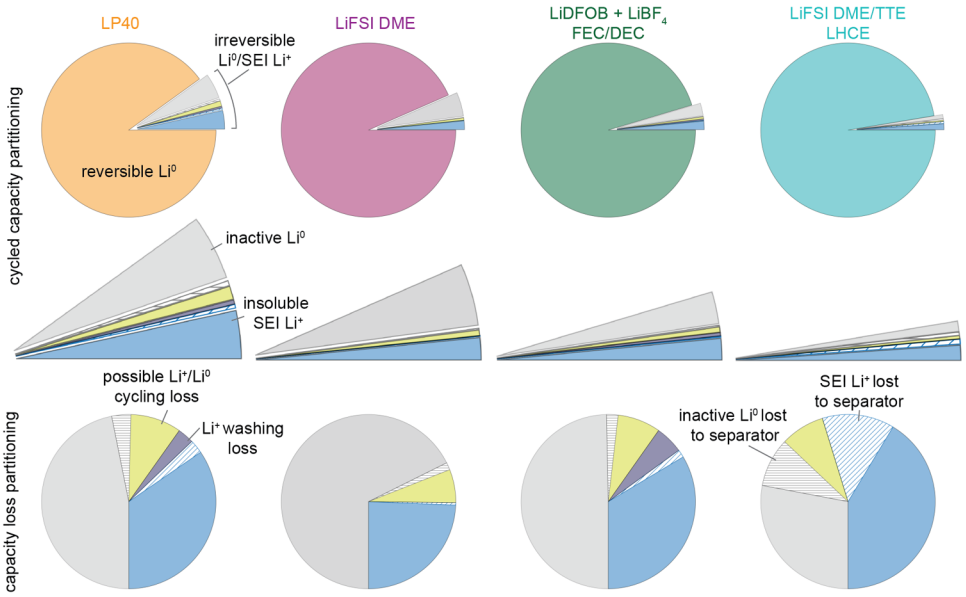

Figure 3. Partitioning of capacity in each of the tested electrolytes, with accounting updated to include previously unresolved material lost to disassembly and washing steps.

understood by including an estimate of SEI Li^+ lost to the separator. This value was estimated by assuming that the ratio of inactive Li^0 to SEI Li^+ on the separator is the same as on the Cu WE (Figure S8). After accounting for the additional projected SEI losses to the separator, reasonable agreement is achieved between the potentiostat capacity loss and the inventoried residual materials in the two ether-based electrolytes (LiFSI DME and LiFSI DME/TTE LHCE). However, a shortfall still exists for the other two carbonate-based electrolytes.

To investigate whether the remaining missing Li^+ can be attributed to sample handling, we examined the impacts of the washing process in greater detail by conducting NMR on the wash solvent—dimethyl carbonate (DMC) for carbonate-based electrolytes and DME for ether-based electrolytes—to quantify dissolved Li^+-containing species. To distinguish between artifact electrolyte salt and possible Li^+ species dissolved during washing, ^{19}F-NMR was used to quantify the electrolyte anions (A^-) present, ^{7}Li NMR was used to quantify the total Li^+ in solution, and the concentration of Li^+ species dissolved during washing was estimated by subtracting the two:

$$[Li^+_{dissolved\ during\ wash}] = [Li^+_{total}] - [A^-] \quad (1)$$

This analysis confirmed that the LiFSI DME and LHCE electrolytes had essentially zero losses to solubility in the wash solvent (Figure S10a), which is consistent with the good agreement obtained between potentiostat and accounted-for residuals in Figure 2b. However, in LP40 and LiDFOB + $LiBF_4$ FEC/DEC, a relatively minor though nonzero quantity of Li^+—approximately 0.03 and 0.04 mAh, respectively—was dissolved during washing (Figure S10a). Notably, changing the identity of the particular polar aprotic wash solvent (DMC, DME, or THF) did not impact recovery fraction as exemplified for the LP40 sample (Figure S10b).

Overall, after accounting for the material on the Cu WE, the separator, and the wash solvent for all electrolytes, with appropriate error propagation, the total assignable residual material is within error, although still systematically below, the total capacity loss for all electrolytes (Figure 2b). The only remaining route for material loss is thus to SEI dissolution or physical dislodgment of Li^+/Li^0-containing material during active cell cycling, such that it is nonrecoverable from either the Cu WE or the separator. While it is difficult to probe this quantitatively, qualitative ^{1}H NMR was conducted on cycled electrolytes. Three electrolytes showed no additional chemical signatures after cycling, though LP40 had a new ^{1}H NMR singlet at 4.3 ppm (Figure S11), which has been previously observed in cycled carbonate electrolytes and assigned to lithium ethylene decarbonate (LEDC).[27] This result indicates that among the examined electrolytes, LP40 exhibits the most meaningful losses to Li^+ solubility during cycling.

The updated understanding of capacity loss afforded by these additional quantifications is displayed in Figure 3. Overall, the most important takeaways are as follows. First, if only inactive Li^0 is of interest, with no separator removal or washing, then the only potential loss mode that needs to be considered relates to material loss during cell cycling (citron-colored wedge). As discussed above, these losses are a minor portion of total capacity loss, confirming that in unwashed samples the practice of assigning all noninactive Li^0 losses to insoluble SEI Li^+ is a reasonable assumption. For SEI analysis on washed samples, these measurements reveal that the phenomena driving incomplete Li inventory vary between electrolyte chemistries. Among the electrolytes studied here, separator losses are most pronounced in the LHCE (Figure S6) but are otherwise very minor. Meanwhile, carbonate electrolytes appear to generate the most soluble SEI, and hence have the greatest losses to washing. Overall, it must be emphasized that in all cases, separator removal and washing still permit a majority of material to be inventoried. Having now assigned these previously unresolved portions of capacity loss, we can finally investigate their impact on the interpretation of SEI quantification results.

Quantified SEI species are usually normalized for ease of comparison between electrolytes, either by dividing by the potentiostat-measured capacity loss[7] or the total Li^0/Li^+ on Cu WE as measured by ICP or NMR.[6,18] The latter approach is only an option for washed samples, because salt residue must

https://doi.org/10.1021/acsenergylett.5c01274
ACS Energy Lett. 2025, 10, 4269−4276

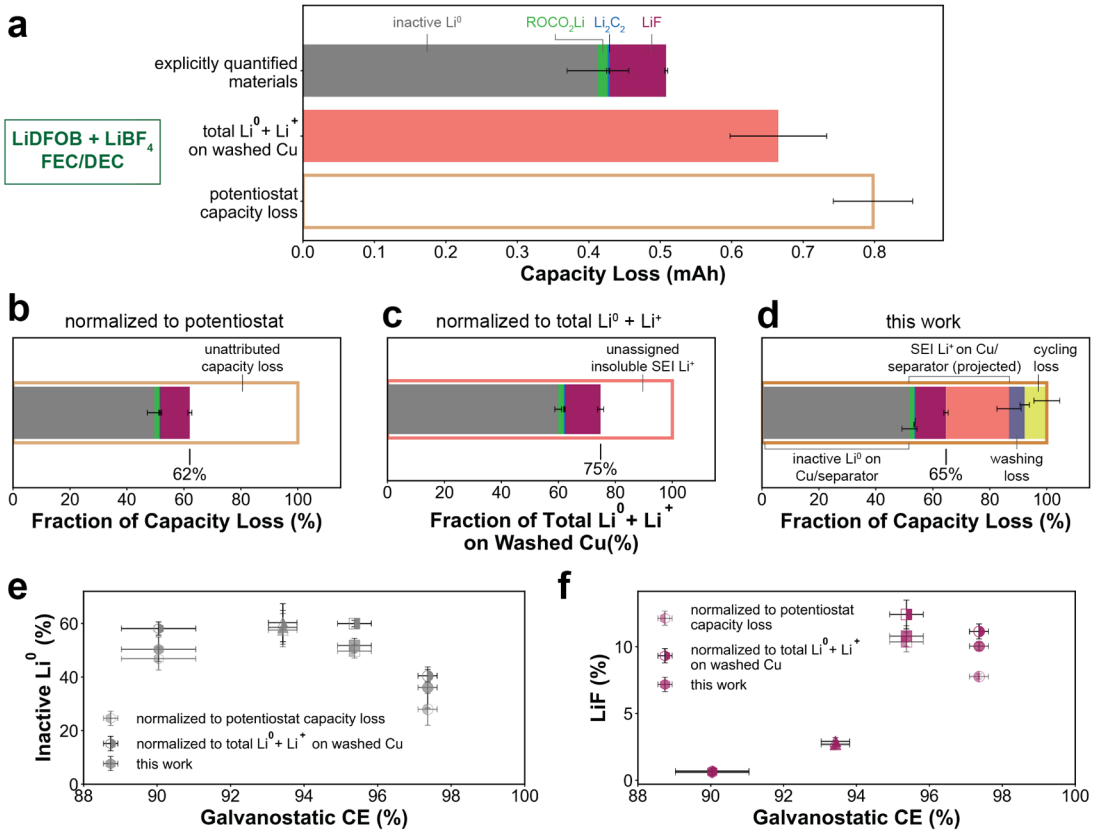

Figure 4. Investigating the impact of improved Li^0/Li^+accounting on the interpretation of quantification data. (a) Explicitly quantified Li-containing residual materials on washed Cu WE plotted alongside potentiostat capacity loss for LiDFOB + $LiBF_4$ FEC/DEC electrolyte. For this electrolyte, (b) quantified materials normalized to total capacity loss; (c) quantified materials normalized to total Li^0 + Li^+ on washed Cu WE; and (d) quantified materials scaled to include separator losses and plotted with the measured Li^+ washing losses, normalized to potentiostat capacity loss. (e) Inactive Li^0 and (f) LiF quantification results for all electrolytes plotted vs. CE using each data processing approach. For all plots, bar length or data point location is the mean value, with error bars denoting one standard deviation, $n \geq 3$. For (e) and (f), symbol shape corresponds to the electrolyte: hexagons for LP40, triangles for LiFSI DME, squares for LiDFOB + $LiBF_4$ FEC/DEC, and circles for the LiFSI DME/TTE LHCE electrolyte.

be removed to accurately quantify the total Li inventory (Figure S12). Here, we investigated the impact of different normalization choices on conclusions one would reach by measuring three representative SEI species ($ROCO_2Li$, Li_2C_2, and LiF, see Note S4) and Li^0 in the four electrolytes examined here, then normalizing by the different options indicated above. Detailed quantification and normalization results are shown for the LiDFOB + $LiBF_4$ FEC/DEC electrolyte in Figure 4a-d, and for all other electrolytes in Figure S13. Due to the difference between the potentiostat-measured capacity loss and the total Li^0 + Li^+ measured by ICP, the percentage of explicitly quantified materials for the LiDFOB + $LiBF_4$ FEC/DEC electrolyte varies between the two approaches: 62% vs 75%, respectively (Figure 4b-c). The other electrolytes also show slight differences in material inventory between quantification schemes, with the LHCE electrolyte exhibiting the greatest discrepancy (36% vs. 52%) because it has the lowest Li recovery fraction on the washed Cu WE (Figure S13b-c). Armed with the measurements performed in this work, we can navigate these differences by calculating a "more informed" estimate, which accounts for each mode of material loss documented here (Figure 4d). To do this, the SEI phases in the separator are assumed to be proportional to what was directly measured on the Cu electrode (Supporting Information Methods) and all materials are normalized to the potentiostat capacity loss. This adjusts the total quantified materials to 65% in the LiDFOB + $LiBF_4$ FEC/DEC electrolyte, and 47% in the LHCE. Notably, though exact values vary somewhat, the trends in SEI composition across electrolytes are not significantly impacted by the normalization scheme: e.g. LiFSI DME/TTE LHCE has the lowest proportion of inactive Li^0 (Figure 4e), and LiDFOB + $LiBF_4$ FEC/DEC has the greatest quantity of LiF (Figure 4f) in all cases. This observation emphasizes the particular strength of performing SEI capacity loss analyses across multiple electrolytes to interpret larger trends, ideally with suitable statistical analysis,[7] which is robust to minor material losses; however it also exemplifies that percentages of a specific sample must be presented and interpreted with appropriate caution.

As a whole, this work offers new insights into the mapping of capacity losses of Li metal anodes. By conducting detailed measurements of material losses during sample processing, the material balance on Li-containing residuals was brought within error of the total capacity loss in four different electrolytes. The impacts of sample processing were found to be electrolyte chemistry-dependent, but ultimately, broader conclusions related to SEI composition and inactive Li^0 quantification were qualitatively unaffected by this improved accounting of Li residuals. However, in cases when the research question centers on the SEI composition of a particular electrolyte

https://doi.org/10.1021/acsenergylett.5c01274
ACS Energy Lett. 2025, 10, 4269−4276

system, rather than larger trends across multiple electrolytes, the best practice is to measure and report a Li recovery fraction whenever possible. Additionally, the roadmap for capacity loss accounting presented here may be particularly useful as SEI quantification techniques are adapted to Na anodes, where SEI solubility during cycling is expected to represent a greater proportion of capacity loss,[28,29] and in full-cell conditions, where oxidative electrolyte decomposition has been shown to generate protic species which damage SEI stability and accelerate capacity loss.[30,31] In full, this study affirms the reliability of quantitative capacity loss analysis techniques at Li metal anodes, and offers a more stringent approach to tracking material losses when quantitative inventory is of particular concern.

■ ASSOCIATED CONTENT

Supporting Information

The Supporting Information is available free of charge at https://pubs.acs.org/doi/10.1021/acsenergylett.5c01274.

Experimental methods; additional details about sample preparation process; comparison of results between different laboratories and experimentalists; additional representations of data plotted in main text figures; ^{1}H NMR on cycled electrolytes; a detailed description of calculations applied during data analysis; and four supporting discussion notes expanding upon experimental methodology, deposit morphology observations, and generalizing findings to more diverse electrolytes (PDF)

■ AUTHOR INFORMATION

Corresponding Author

Betar M. Gallant − *Department of Mechanical Engineering, Massachusetts Institute of Technology, Cambridge, Massachusetts 02139, United States; Energy Storage Research Alliance, Argonne National Laboratory, Lemont, Illinois 60439, United States;* orcid.org/0000-0002-4586-2769; Email: bgallant@mit.edu

Authors

Katherine Steinberg − *Department of Chemical Engineering, Massachusetts Institute of Technology, Cambridge, Massachusetts 02139, United States; Energy Storage Research Alliance, Argonne National Laboratory, Lemont, Illinois 60439, United States;* orcid.org/0000-0002-8232-7714

Wurigumula Bao − *Pritzker School of Molecular Engineering, University of Chicago, Chicago, Illinois 60637, United States; Energy Storage Research Alliance, Argonne National Laboratory, Lemont, Illinois 60439, United States;* orcid.org/0000-0001-8109-1546

Kun Ryu − *Pritzker School of Molecular Engineering, University of Chicago, Chicago, Illinois 60637, United States; Energy Storage Research Alliance, Argonne National Laboratory, Lemont, Illinois 60439, United States*

Ying Shirley Meng − *Pritzker School of Molecular Engineering, University of Chicago, Chicago, Illinois 60637, United States; Department of NanoEngineering, University of California San Diego, San Diego, California 92093, United States; Energy Storage Research Alliance, Argonne National Laboratory, Lemont, Illinois 60439, United States;* orcid.org/0000-0001-8936-8845

Complete contact information is available at: https://pubs.acs.org/10.1021/acsenergylett.5c01274

Notes

The authors declare no competing financial interest.

■ ACKNOWLEDGMENTS

This work is funded by the Energy Storage Research Alliance "ESRA" (DE-AC02-06CH11357), an Energy Innovation Hub funded by the U.S. Department of Energy, Office of Science, Basic Energy Sciences. This work was carried out in part through the use of MIT.nano's facilities, and also made use of the MIT Department of Chemistry Instrumentation Facility.

■ REFERENCES

(1) Hobold, G. M.; Lopez, J.; Guo, R.; Minafra, N.; Banerjee, A.; Shirley Meng, Y.; Shao-Horn, Y.; Gallant, B. M. Moving beyond 99.9% Coulombic efficiency for lithium anodes in liquid electrolytes. *Nat. Energy* **2021**, *6* (10), 951−960.

(2) Yoshimatsu, I.; Hirai, T.; Yamaki, J.-i. Lithium Electrode Morphology during Cycling in Lithium Cells. *J. Electrochem. Soc.* **1988**, *135* (10), 2422−2427.

(3) Peled, E. The Electrochemical Behavior of Alkali and Alkaline Earth Metals in Nonaqueous Battery Systems—The Solid Electrolyte Interphase Model. *J. Electrochem. Soc.* **1979**, *126* (12), 2047−2051.

(4) Tasaki, K.; Goldberg, A.; Lian, J.-J.; Walker, M.; Timmons, A.; Harris, S. J. Solubility of Lithium Salts Formed on the Lithium-Ion Battery Negative Electrode Surface in Organic Solvents. *J. Electrochem. Soc.* **2009**, *156* (12), A1019−A1019.

(5) Fang, C.; Li, J.; Zhang, M.; Zhang, Y.; Yang, F.; Lee, J. Z.; Lee, M. H.; Alvarado, J.; Schroeder, M. A.; Yang, Y.; et al. Quantifying inactive lithium in lithium metal batteries. *Nature* **2019**, *572* (7770), 511−515.

(6) Hobold, G. M.; Gallant, B. M. Quantifying Capacity Loss Mechanisms of Li Metal Anodes beyond Inactive Li-0. *ACS Energy Lett.* **2022**, *7* (10), 3458−3466.

(7) Hobold, G. M.; Wang, C.; Steinberg, K.; Li, Y.; Gallant, B. M. High lithium oxide prevalence in the lithium solid-electrolyte interphase for high Coulombic efficiency. *Nat. Energy* **2024**, *9* (5) 580591.

(8) McShane, E. J.; Colclasure, A. M.; Brown, D. E.; Konz, Z. M.; Smith, K.; McCloskey, B. D. Quantification of Inactive Lithium and Solid-Electrolyte Interphase Species on Graphite Electrodes after Fast Charging. *ACS Energy Letters* **2020**, *5* (6), 2045−2051.

(9) Sayahpour, B.; Li, W.; Bai, S.; Lu, B.; Han, B.; Chen, Y. T.; Deysher, G.; Parab, S.; Ridley, P.; Raghavendran, G.; et al. Quantitative analysis of sodium metal deposition and interphase in Na metal batteries. *Energy Environ. Sci.* **2024**, *17* (3), 1216−1228.

(10) Fang, C.; Lu, B.; Pawar, G.; Zhang, M.; Cheng, D.; Chen, S.; Ceja, M.; Doux, J.-M.; Musrock, H.; Cai, M.; et al. Pressure-tailored lithium deposition and dissolution in lithium metal batteries. *Nat. Energy* **2021**, *6* (10), 987−994.

(11) Ding, J. F.; Xu, R.; Xiao, Y.; Zhang, S.; Song, T. L.; Yan, C.; Huang, J. Q. Dynamic Galvanic Corrosion of Working Lithium Metal Anode Under Practical Conditions. *Adv. Energy Mater.* **2023**, *13* (21), 2204305.

(12) Lu, B.; Olivera, E.; Scharf, J.; Chouchane, M.; Fang, C.; Ceja, M.; Pangilinan, L. E.; Zheng, S.; Dawson, A.; Cheng, D.; et al. Quantitatively Designing Porous Copper Current Collectors for Lithium Metal Anodes. *ACS Applied Energy Materials* **2021**, *4* (7), 6454−6465.

(13) Lu, B.; Li, W.; Cheng, D.; Bhamwala, B.; Ceja, M.; Bao, W.; Fang, C.; Meng, Y. S. Suppressing Chemical Corrosions of Lithium Metal Anodes. *Adv. Energy Mater.* **2022**, *12* (48), 2202012.

(14) Xiang, Y.; Tao, M.; Chen, X.; Shan, P.; Zhao, D.; Wu, J.; Lin, M.; Liu, X.; He, H.; Zhao, W.; et al. Gas induced formation of inactive Li in rechargeable lithium metal batteries. *Nat. Commun.* **2023**, *14*, 177.

(15) Pal, U.; Rakov, D.; Lu, B.; Sayahpour, B.; Chen, F.; Roy, B.; MacFarlane, D. R.; Armand, M.; Howlett, P. C.; Meng, Y. S.; et al. Interphase control for high performance lithium metal batteries using ether aided ionic liquid electrolyte. *Energy Environ. Sci.* **2022**, *15* (5), 1907−1919.
(16) Weret, M. A.; Jiang, S. K.; Shitaw, K. N.; Chang, C. Y.; Tekaligne, T. M.; Chiou, J. C.; Yang, S. C.; Temesgen, N. T.; Nikodimos, Y.; Wu, S. H.; et al. Reviving Inactive Lithium and Stabilizing Lithium Deposition for Improving the Performance of Anode-Free Lithium-Sulfur Batteries. *ACS Energy Letters* **2023**, *8* (6), 2817−2823.
(17) Zhang, W.; Sayavong, P.; Xiao, X.; Oyakhire, S. T.; Shuchi, S. B.; Vilá, R. A.; Boyle, D. T.; Kim, S. C.; Kim, M. S.; Holmes, S. E.; et al. Recovery of isolated lithium through discharged state calendar ageing. *Nature* **2024**, *626* (7998), 306−312.
(18) Steinberg, K.; Gallant, B. M. Revealing the Role of Lithium Carbonate at Lithium Metal Anodes Through Study of Gas-Reacted Interphases. *J. Electrochem. Soc.* **2024**, *171*, 080530.
(19) Bao, W.; Fang, C.; Cheng, D.; Zhang, Y.; Lu, B.; Tan, D. H. S.; Shimizu, R.; Sreenarayanan, B.; Bai, S.; Li, W.; et al. Quantifying lithium loss in amorphous silicon thin-film anodes via titration-gas chromatography. *Cell Reports Physical Science* **2021**, *2* (10), 100597.
(20) Sreenarayanan, B.; Tan, D. H. S.; Bai, S.; Li, W.; Bao, W.; Meng, Y. S. Quantification of Lithium Inventory Loss in Micro Silicon Anode via Titration-Gas Chromatography. *J. Power Sources* **2022**, *531*, 231327.
(21) Tan, D. H. S.; Chen, Y.-T.; Yang, H.; Bao, W.; Sreenarayanan, B.; Doux, J.-M.; Li, W.; Lu, B.; Ham, S.-Y.; Sayahpour, B.; et al. Carbon-free high-loading silicon anodes enabled by sulfide solid electrolytes. *Science* **2021**, *373* (6562), 1494−1499.
(22) Hirsh, H. S.; Sayahpour, B.; Shen, A.; Li, W.; Lu, B.; Zhao, E.; Zhang, M.; Meng, Y. S. Role of electrolyte in stabilizing hard carbon as an anode for rechargeable sodium-ion batteries with long cycle life. *Energy Storage Mater.* **2021**, *42*, 78−87.
(23) Oh, J. A. S.; Deysher, G.; Ridley, P.; Chen, Y. T.; Cheng, D.; Cronk, A.; Ham, S. Y.; Tan, D. H. S.; Jang, J.; Nguyen, L. H. B.; et al. High-Performing All-Solid-State Sodium-Ion Batteries Enabled by the Presodiation of Hard Carbon. *Adv. Energy Mater.* **2023**, *13* (26), 2300776.
(24) Parimalam, B. S.; MacIntosh, A. D.; Kadam, R.; Lucht, B. L. Decomposition Reactions of Anode Solid Electrolyte Interphase (SEI) Components with LiPF6. *J. Phys. Chem. C* **2017**, *121* (41), 22733−22738.
(25) Weber, R.; Genovese, M.; Louli, A. J.; Hames, S.; Martin, C.; Hill, I. G.; Dahn, J. R. Long cycle life and dendrite-free lithium morphology in anode-free lithium pouch cells enabled by a dual-salt liquid electrolyte. *Nature Energy* **2019**, *4* (8), 683−689.
(26) Ren, X.; Zou, L.; Cao, X.; Engelhard, M. H.; Liu, W.; Burton, S. D.; Lee, H.; Niu, C.; Matthews, B. E.; Zhu, Z.; et al. Enabling High-Voltage Lithium-Metal Batteries under Practical Conditions. *Joule* **2019**, 3 (7), 1662−1676.
(27) Jin, Y.; Kneusels, N. J. H.; Magusin, P. C. M. M.; Kim, G.; Castillo-Martínez, E.; Marbella, L. E.; Kerber, R. N.; Howe, D. J.; Paul, S.; Liu, T.; et al. Identifying the Structural Basis for the Increased Stability of the Solid Electrolyte Interphase Formed on Silicon with the Additive Fluoroethylene Carbonate. *J. Am. Chem. Soc.* **2017**, *139* (42), 14992−15004.
(28) Ma, L. A.; Naylor, A. J.; Nyholm, L.; Younesi, R. Strategies for Mitigating Dissolution of Solid Electrolyte Interphases in Sodium-Ion Batteries. *Angewandte Chemie - International Edition* **2021**, *60* (9), 4855−4863.
(29) Mogensen, R.; Brandell, D.; Younesi, R. Solubility of the Solid Electrolyte Interphase (SEI) in Sodium Ion Batteries. *ACS Energy Letters* **2016**, *1* (6), 1173−1178.
(30) Bao, W.; Yao, W.; Li, Y.; Sayahpour, B.; Han, B.; Raghavendran, G.; Shimizu, R.; Cronk, A.; Zhang, M.; Li, W.; et al. Insights into lithium inventory quantification of LiNi0.5Mn1.5O4-graphite full cells. *Energy Environ. Sci.* **2024**, *17* (12), 4263−4272.
(31) Kwon, Y.; Svirinovsky-Arbeli, A.; Hestenes, J. C.; Buitrago Botero, P. J.; Corpus, K. R. M.; Lepucki, P.; Pecher, O.; Marbella, L. E. Elucidating the role of cathode identity: Voltage-dependent reversibility of anode-free batteries. *Chem.* **2024**, *10* (10), 3159−3183.

https://doi.org/10.1021/acsenergylett.5c01274
ACS Energy Lett. 2025, 10, 4269−4276